Simulation and fabrication of attenuated phase-shifting masks: CrF_x

Eunah Kim, Seungbum Hong, Kyong-Sub Kim, Zhong-Tao Jiang, Dae Weon Kim, Sungchul Lim, Sang-Gyun Woo, Young-Bum Koh, and Kwangsoo No

To acquire the required resolution for 248- and 193-nm lithography, a study of attenuated phase-shifting mask (Att-PSM) technology is in progress. We performed a simulation study using a matrix method to calculate relative transmittance and the amount of phase shift of light through the PSM. However, we found that the average film composition changed with deposition time. Accordingly, optical constants were found to be a strong function of film thickness. Therefore we rearranged the relationship between deposition parameters (e.g., deposition time or gas flow rate ratio) and optical constants (e.g., refractive index and extinction coefficient) to extract the empirical formula for the optical constants with respect to film composition. To verify our simulation study, we fabricated a phase shifter based on our simulation result, which was found to have a transmittance of 8.3% and a phase shift of 179.5°. Consequently, we obtained a reliable optimum condition for the deep-ultraviolet Att-PSM. © 1997 Optical Society of America

Key words: Phase-shifting mask, attenuated type, chromium–fluoride.

1. Introduction

A phase-shifting mask (PSM) is a mask that changes the phase of light to cause destructive interference at the edge with an original light (Subsection 2.A). It has been reported[1] that it may be the most desirable device for enhancing optical lithography in the very large-scale integrated/very-high-speed-integrated-circuit era. The use of a PSM improves both resolution and depth of focus without significantly altering the existing exposure system. This phase-shifting technology is expected to extend the use of the conventional system in fabrications of gigadynamic RAM with a minimum feature size of ~0.18 μm.

It is known[2] that Cr-based materials are strong candidates for attenuated phase-shifting mask (Att-PSM) materials because of their excellent etch selectivity with respect to fused silica substrates in the $Cl_2 + O_2$ mixture gas during Reactive Ion Etching. However, it has been found that most Cr-based materials show low transmittance in the deep-UV region. To overcome this low-transmittance problem, we substituted the anions of a Cr compound with fluorine atoms having high electronegativity. To verify the applicability of CrF_x film as an Att-PSM material, we performed both a simulation and an experimental study.

To date, there have been many research activities centered around an Att-PSM condition simulation. Ito *et al.*[3] performed a simulation of the Att-PSM condition, considering the multiple reflection inside the film. However, it is also necessary to consider the multiple reflection within the substrate, since the finite substrate thickness affects the phase shift and the intensity of the light in a significant way. Tanabe *et al.*[4] used the RT method, that is, fitting the measurement data of the reflectance and the transmittance to the calculated one, by the nonlinear least-squares method, to obtain refractive index n and extinction coefficient k. Based on their findings, they calculated the phase shift.[4] However, according to our experiments, film composition is dependent on film thickness. Since optical constants (such as n and k) are considered to be a function of film composition, it is found that they are again a function of film thickness. Therefore, for an optimum Att-PSM condition, the re-

E. Kim, S. Hong, K.-S. Kim, Z.-T. Jiang, D. W. Kim, and K. No are with the Department of Materials Science and Engineering, Korea Advanced Institute of Science and Technology, Taejon, Korea. S. Lim, S.-G. Woo, and Y.-B. Koh are with the Samsung Electronics Company, Ltd., Yongin, Kyongki-do, Korea.

Received 17 January 1997; revised manuscript received 13 May 1997.
0003-6935/97/287247-10$10.00/0
© 1997 Optical Society of America

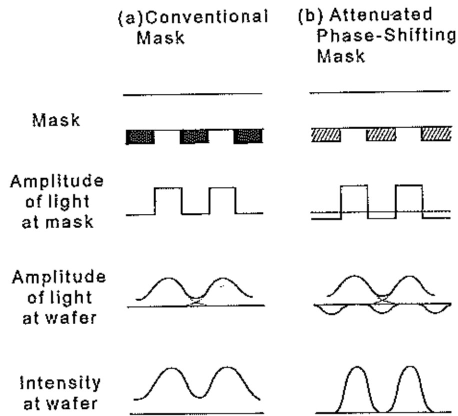

Fig. 1. Comparison of imaging through an attenuated PSM and a conventional mask.

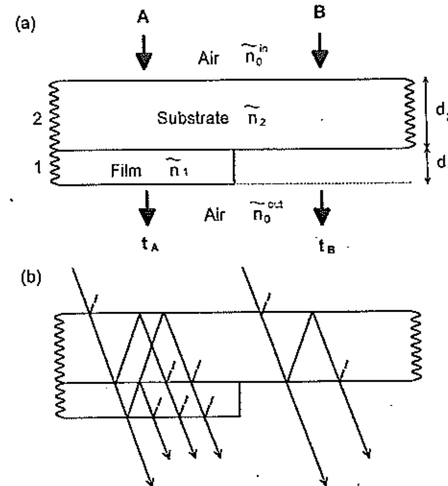

Fig. 2. Basic model of the simulation study: (a) optical parameters used in this simulation, (b) the phenomena of multiple reflection.

lationship between optical constants and the thickness should be considered in the simulation.

Also, note that the air layer having the same thickness as the film should be taken into account for a reference light. This is explained in Subsection 2.B.

In this study, we performed a simulation study to find the optimum Att-PSM fabrication condition, considering the following factors:

(1) The multiple reflection within both the film and the substrate.

(2) The dependence of the optical constants on film thickness.

(3) The air layer of the same thickness with the film.

To verify this simulation study, we fabricated CrF_x masks in different conditions and measured the transmittance, phase shift, film thickness, and film composition.

2. Theoretical Background and Simulation Study of the Phase-Shifting Masks

A. Basic Concept of Attenuated Phase-Shifting Masks

Light is an electromagnetic wave, characterized by wavelength, amplitude, and phase. Shifting the phase by 180° is equivalent to changing the sign of the amplitude. A conventional chrome transmission mask consisting of clear and opaque areas controls only the passage of the light, not the magnitude of the amplitude and its sign. An Att-PSM, on the other hand, controls both amplitude and phase.

The conventional mask and the Att-PSM are schematically illustrated in Fig. 1. In the case of the Att-PSM [Fig. 1(b)], light passing through a phase shifter of thickness $d = 0.5\lambda/(n - 1)$ (n is the refractive index of the shifter material and λ is the exposure wavelength) reverses its amplitude at the mask, that is, changes phase by 180°. The intensity of the light also changes to show a transmittance of 5–10%.

The amplitude profile at the plane of the transmission mask consists of square-wave features. Relative phases are unchanged by passage through the optical tool, which acts as a spatial low-pass filter, passing only the first-order diffracted beam near the resolution limit of the exposure tool and resulting in degradation (broadening and rounding) of the amplitude pattern associated with each aperture. The resulting amplitude pattern at the wafer plane is the algebraic sum of the degraded amplitude from each aperture. The intensity at the wafer plane is simply the absolute square of the resultant amplitude and is not dependent on sign. As we approach the resolution limit of the exposure tool, the constructive interference of the overlapping amplitude functions in the center of the dark feature significantly deteriorates the contrast in the optical image, as shown in the resultant intensity profile[5] [Fig. 1(a)].

In comparison, the amplitude of the square-wave pattern at the mask plane for the Att-PSM consists of positive and attenuated negative features in alternating patterns. Passage through the optical tool again degrades the amplitude profile, but, because adjacent profiles are 180° out of phase, the amplitude in the overlapped area is significantly reduced and the resulting contrast in the intensity profile is significantly enhanced over that produced by the non-phase-shifting mask. Moreover the light passing through the phase shifter experiences intensity attenuation to as low as 5–10% so as not to cause photoreaction inside the photoresist, which leads to the creation of ghost lines.[6] The net result is a significant increase in contrast for fine dark features.

In summary, the required Att-PSM condition is a 180° phase shift and a transmittance attenuation of 5–10% at the exposure wavelength.

B. Transmittance and Phase-Shift Simulation

The basic model that we adopted for this simulation study is shown in Fig. 2. If electromagnetic radiation falls onto a structure consisting of thin layers of different materials (such as film + substrate in Fig.

2), multiple reflections take place within the structure [Fig. 2(b)]. Depending on the light source and the layer thickness, reflected beams may be coherent and interfere with one another.

Consider two systems, A and B, consisting of two layers, as shown in Fig. 2. The construction parameters comprise not only the complex refractive index $\tilde{n}_j$ and the thickness d_j of the layers $j = 1, 2$ but also the complex refractive indices $\tilde{n}_0^{\text{in}}$ and $\tilde{n}_0^{\text{out}}$ of the air medium:

$$\tilde{n}_j = n_j - ik_j, \tag{1}$$

where n_j is the refractive index of the jth layer and k_j is the extinction coefficient of the jth layer;

$$\tilde{n}_0 = n_0 - ik_0 = n_0 = 1, \tag{2}$$

where n_0 is the refractive index of the air layer and k_0 is the extinction coefficient of the air layer.

Here we consider only the case where the angle of incidence is zero (normal to the substrate plane), because the exposure system is almost normal to the mask.

The most general method of calculating the transmittance T and the phase shift φ of a multilayered structure is based on a matrix formulation of the boundary condition at the film surface derived from Maxwell's equations.[7]

It can be shown that the transmittance coefficient of the above systems A and B bound by semi-infinite media is given by

$$t_S = \frac{2\tilde{n}_0^{\text{in}}}{\tilde{n}_0^{\text{in}}\,\mathbf{E}_0^{\text{in}} + \mathbf{H}_0^{\text{in}}}, \tag{3}$$

where S = A, B and

$$\begin{pmatrix} \mathbf{E}_0^{\text{in}} \\ \mathbf{H}_0^{\text{in}} \end{pmatrix} = M_S \begin{pmatrix} 1 \\ \tilde{n}_0^{\text{out}} \end{pmatrix}, \tag{4}$$

where $\mathbf{E}_0^{\text{in}}$ and $\mathbf{H}_0^{\text{in}}$ are the electric and the magnetic field vectors, respectively, in the incident medium and M_S is a product matrix given by

$$M_S = M_2 M_1. \tag{5}$$

In the preceding equation, M_j is a 2×2 matrix that represents the jth layer of the system:

$$M_j = \begin{pmatrix} \cos\delta_j & \dfrac{i}{\tilde{n}_j}\sin\delta_j \\ i\tilde{n}_j \sin\delta_j & \cos\delta_j \end{pmatrix}, \tag{6}$$

where

$$\delta_j = \frac{2\pi}{\lambda}(\tilde{n}_j d_j). \tag{7}$$

The quantity $\tilde{n}_j d_j$ is the effective optical thickness of the jth layer for a normal path to the surface. Then the intensity transmittance is

$$T_S = |t_S|^2, \tag{8}$$

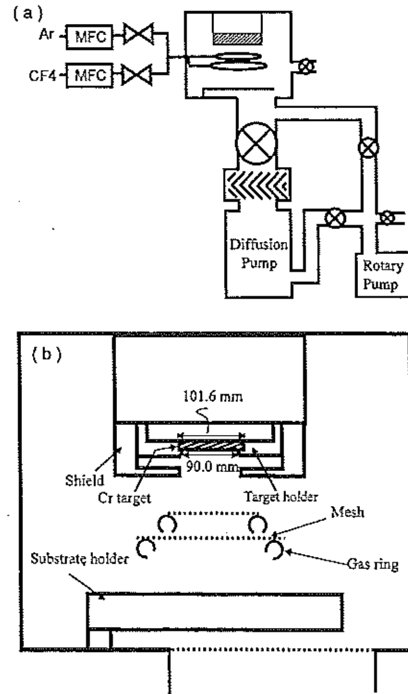

Fig. 3. Schematic diagrams of the dc magnetron sputtering system: (a) all the equipment, (b) inside the chamber.

and the phase shift is given by

$$\phi_S = \arg(t_S). \tag{9}$$

In this calculation, we considered layer 1 of air in Fig. 2(a) to be of the same thickness as the film for the reference light, because the reference light also experiences some amount of phase shift while passing the same distance as the light through the Att-PSM travels. Therefore equations for the relative transmittance and the phase shift with reference to the light passing through the fused silica substrate would be expressed as

$$T = \frac{|t_A|^2}{|t_B|^2}, \tag{10}$$

$$\phi = \{\arg(t_A) - \arg(t_B)\} \times \frac{180}{\pi}\ (\text{deg}). \tag{11}$$

3. Experimental Procedure

A. Apparatus

The apparatus used for the deposition of CrF_x films was a dc magnetron sputtering system, which consisted of a vacuum system, a sputtering target, a dc power supply, a substrate holder system, and a gas injection system. A schematic diagram of the magnetron sputtering system is shown in Fig. 3. We used a dc magnetron sputtering system because it is widely known to have a high deposition rate, low cost, and high reproducibility. In this study, we used two gas rings and a mesh, not only to improve film uniformity but also to getter the fluorine gas, which has high volatility, near the substrate.[8] The Cr target

Table 1. Deposition Condition of CrF_x Films

Variable	Value
Target	Cr(99.95%)
Base pressure	10^{-6} Torr
Working pressure	5×10^{-3} Torr
Total gas flow rate	10 SCCM
CF_4/Ar gas flow rate ratio	Variable
Deposition time	Variable
Direct current power	109 W
Target–substrate distance	132.4 mm
Substrate temperature	R.T.

was fixed to a Cu electrode with a clamp, and above the target there was a permanent circular magnet to induce a magnetic field. To improve film uniformity, the distance between the target and the substrate was fixed to be the maximum distance of 13.24 cm. The mass flow controller (MKS Company) had a 50-SCCM (cubic centimeter per minute at STP) capacitance. We measured and controlled the chamber pressure, using a convectron gauge and an ion gauge. The power supply was Advanced Energy Company's MDX 1 kW.

B. Deposition Condition of CrF_x Films

Table 1 illustrates the deposition condition of CrF_x films deposited in this study. After each deposition, the chamber was cleaned and baked to ensure high reproducibility, because CrF_x film has high reactivity with water vapor that formed inside the chamber during air venting. The main variables for this study were the Ar/CF_4 flow rate ratio and the deposition time.

C. Measurement

In this study, we measured several film properties, i.e., film thickness, average composition, composition depth profile, refractive index, extinction coefficient, transmittance, and phase shift.

Film thickness was measured by the Tencor alpha step, and the step was made through an organic liftoff process. The film composition in terms of the F/Cr ratio was analyzed by Microspec Company's wavelength dispersive spectrometer (WDS) 3-PC. To investigate the composition depth profile of each film, we used Auger electron spectroscopy (AES), Perkin Elmer Company's SAM 4300. We maintained the initial vacuum state at 1×10^{-10} Torr and analyzed the films with a beam voltage of 5 kV and a current of 300 nA. The modulation voltage was 4 V, and the tilting angle was 30°. The AES depth profiling was performed by 3-keV and 25-mA Ar sputtering with an interval of 0.2 min. Impact density was 380 $\mu A/cm^2$.

We measured the refractive index and the extinction coefficient of CrF_x films at wavelengths between 190 and 620 nm, using Sofra Company's spectroscopic ellipsometer, ESVG. The transmittance of each film was measured by Hewlett Packard UV spectroscopy VECTRA 286-12 at a wavelength range between 190 and 820 nm. The phase shift was measured by an interferometer at wavelengths of 248 and 365 nm.

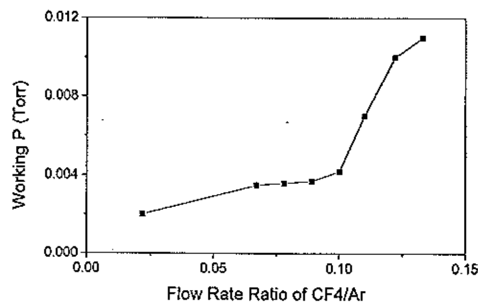

Fig. 4. Dependence of the working pressure on the flow rate ratio of CF_4/Ar.

4. Results and Discussion

A. Gettering Effect

First, we increased the flow rate of CF_4 from 0 to 1.2 SCCM while fixing the Ar flow rate at 9 SCCM. We kept the flow rate constant until the pressure stabilized at each flow rate. Note from Fig. 4 that pressure increases slightly with an increase in the CF_4/Ar flow rate ratio, but, at the flow rate ratio of 0.111, pressure increases abruptly. This phenomenon is explained as follows: Below the critical flow rate ratio, the fluorine getters into the chamber wall and the target so that the amount of reactive gas does not contribute to the chamber pressure. However, above some critical point, the gettering of fluorine reaches a saturation state, so that the increase in the flow rate contributes directly to the chamber pressure.[9]

At the critical flow rate ratio, the target surface changes from a metallic state to a fluoride state, which results in a dramatic decrease in deposition rate. Therefore we chose the deposition flow rate ratio to be between 0.064 and 0.11 to maximize the fluorine incorporation in the film, while at the same time maintaining the target surface metallic state for dc sputtering.

B. Effect of CF_4/Ar Flow Rate Ratio on Film Properties

It was found that the deposition rate was nearly constant, ~1.6 nm/min, when the films were deposited at the chosen flow rate ratio range for 150 min. Figure 5 shows the dependence of the film composition on the CF_4/Ar flow rate ratio analyzed by WDS.

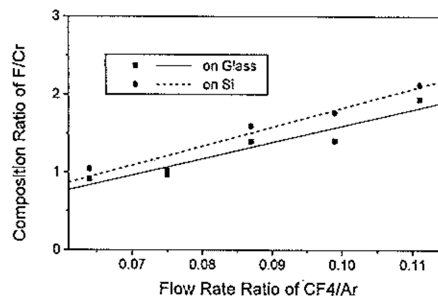

Fig. 5. Dependence of the film composition on the flow rate ratio of CF_4/Ar.

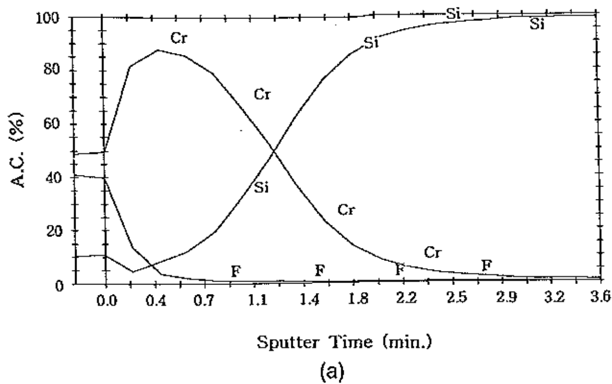

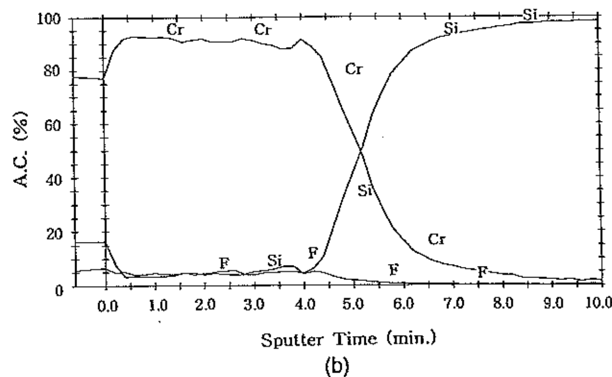

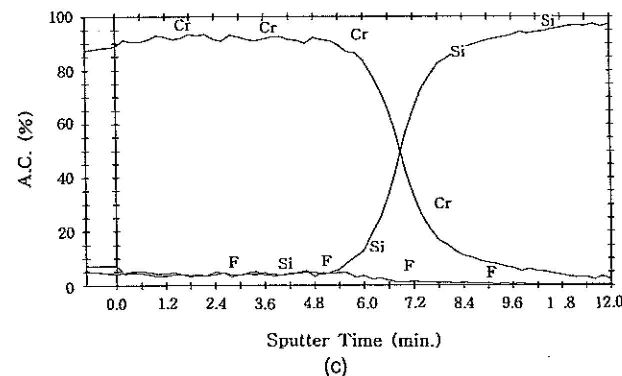

Fig. 6. AES depth profiles of the films. The thicknesses of the films are (a) 84.0, (b) 189.2, and (c) 264.7 nm.

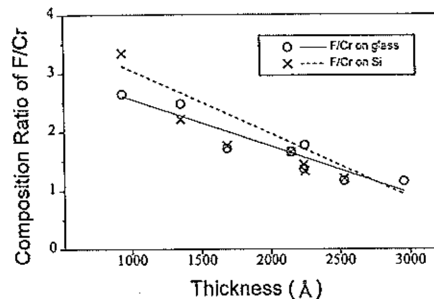

Fig. 7. Dependence of the film composition on the thickness.

The fluorine content increases linearly as the flow rate of CF_4 increases.

C. Dependence of Composition on Film Thickness

Normally the initial growth layer, ~1000 Å thick, is defined as the transition layer, which reflects the structural inhomogeneity in the film thickness direction.[10] Since thin films have steep stress distribution in the thickness direction within the transition layer, the thin film's property is dependent on the thickness. The range of steep stress distribution in thin films is measured as ~1000 Å,[11] and this stress distribution can cause composition distribution. That is, the phase having a lower molar volume is preferred more at the larger tensile stress region and vice versa.

Figure 6 shows the AES depth profiles of films having different thicknesses but deposited in the same conditions except deposition time. As shown in the figure, the fluorine becomes richer at the surface layer as the film thickness decreases. If the film growth rate is higher than the reaction rate, the film composition depends on the growth rate. Therefore the composition should be constant and lower than the equilibrium composition. But, when the film's growth is stopped, the equilibrium phase is formed at the surface layer with diffusion of fluorine. As the film thickness increases, film stress at the surface becomes less tensile. This means that the phase of smaller molar volume is preferred more as the thickness increases. In chromium fluoride cases, the less fluorinated compound has the smaller molar volume. Surface enrichment of fluorine contributes to an average composition shift. So, it is expected that as the thickness increases the average composition is shifted toward a lower fluorine content. Figure 7 shows the WDS analysis results of films with different thicknesses, deposited at the same conditions. The result shows that the average composition (the F/Cr ratio) is shifted toward a lower fluorine content as expected. Accordingly, it can be expected that the optical property of the thin film is a function of thickness. Therefore we considered the dependence of the optical properties on film thickness in this study.

D. Optical Properties

1. *Refractive Index*

Figure 8 shows the dependence of the refractive index on the F/Cr ratio of the films at four different wavelengths: 193, 248, 365, and 436 nm. As can be seen from the figure, the refractive index linearly decreases with an increase in the fluorine content, even though some scatterings of data points are shown. This may be due to the high electron bonding strength of the fluorine, which is considered to decrease the polarizability so as to make the electron cloud shift difficult by the incident electromagnetic wave. This phenomenon is mentioned again in Subsection 4.D.2. We fitted the data points with a linearly decreasing function on the assumption that the refractive index can be expressed as a function of composition only.

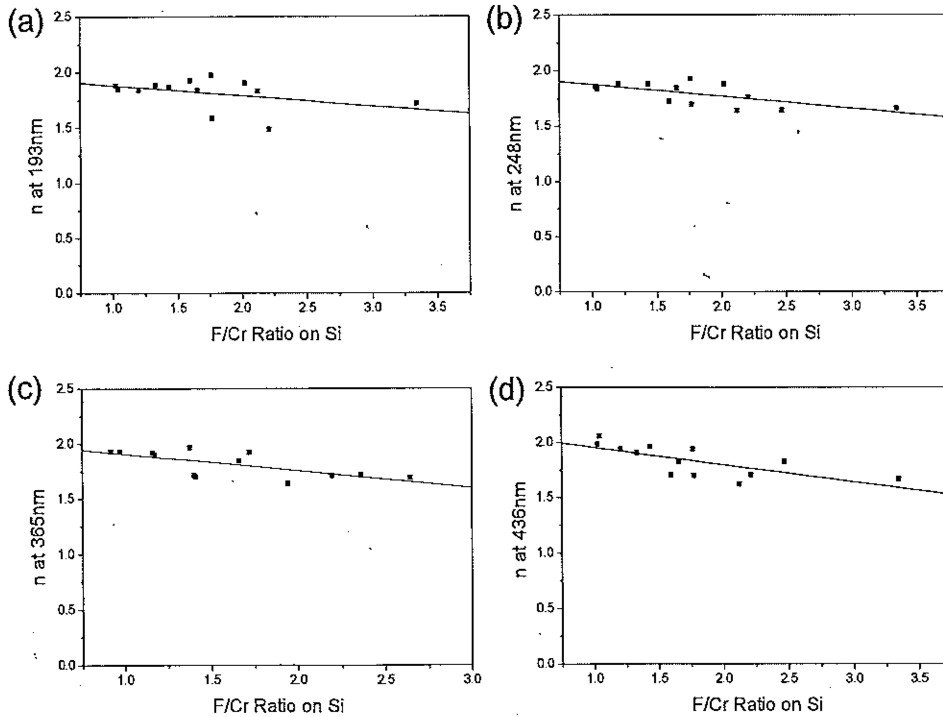

Fig. 8. Dependence of the refractive index on the film composition at four different wavelengths: (a) 193, (b) 248, (c) 365, and (d) 436 nm.

2. *Extinction Coefficient*

In the covalent bonding between two different atoms, one atom attracts the electron pair more strongly than does the other atom. The former is said to be more electronegative. In other words, electronegativity is defined as the atomic property that determines the relative attracting force of the atom over the electron bonded covalently. According to the various calculating methods that determine the relative ability of the bonding atom to attract electrons, several standards of electronegativity were suggested, and the well-known one is that suggested by Pauling.[12] With this standard, the electronegativity of the fluorine, having the highest value of all atoms, is 4.0 (Ref. 12) and that of Cr is 1.6. The richer fluorine in the film causes the smaller extinction co-

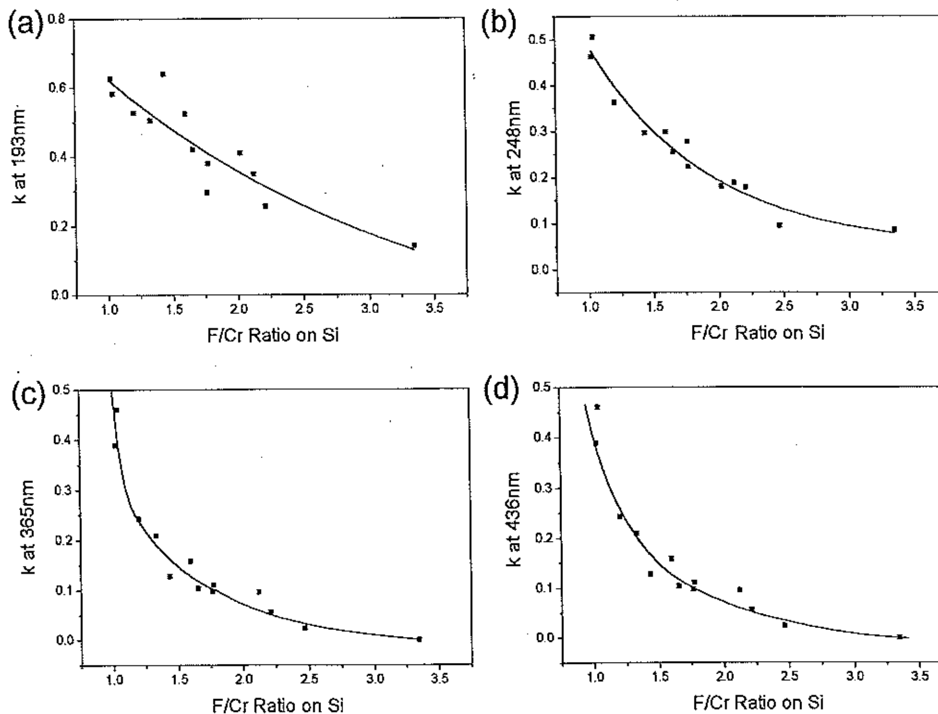

Fig. 9. Dependence of the extinction coefficient on the film composition at four different wavelengths: (a) 193, (b) 248, (c) 365, and (d) 436 nm.

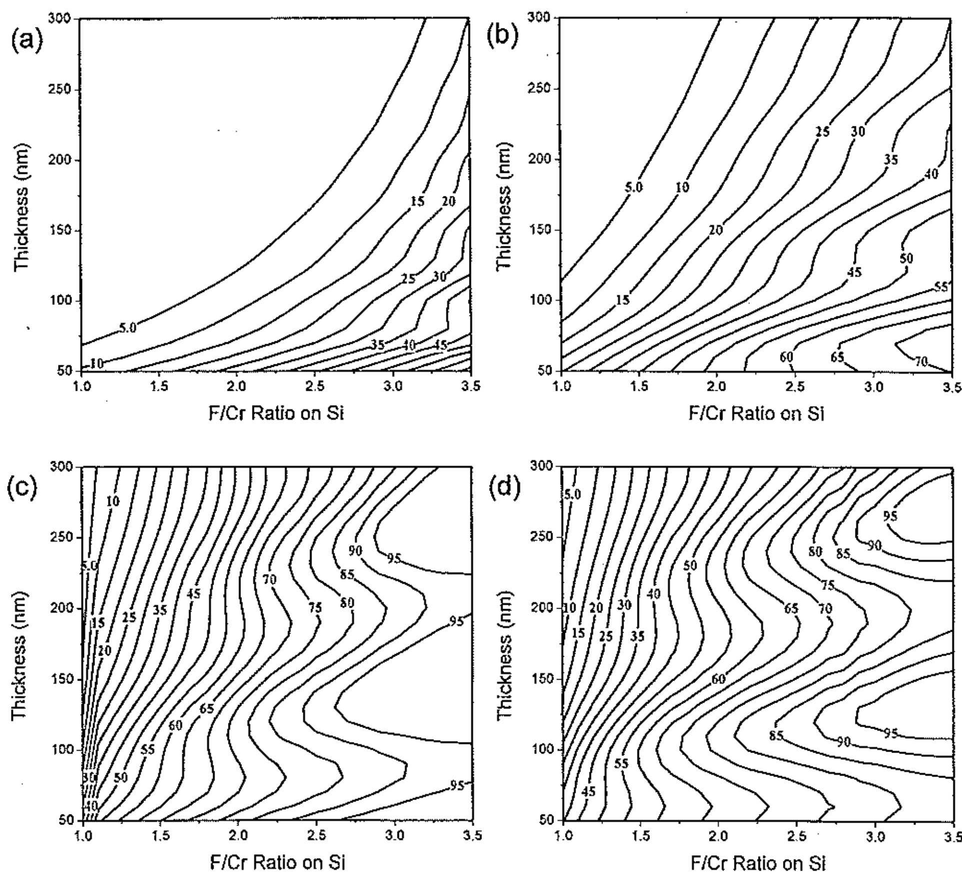

Fig. 10. Simulation of transmittance (numbers in the lines) over film thickness and film composition at wavelengths of (a) 193, (b) 248, (c) 365, and (d) 436 nm.

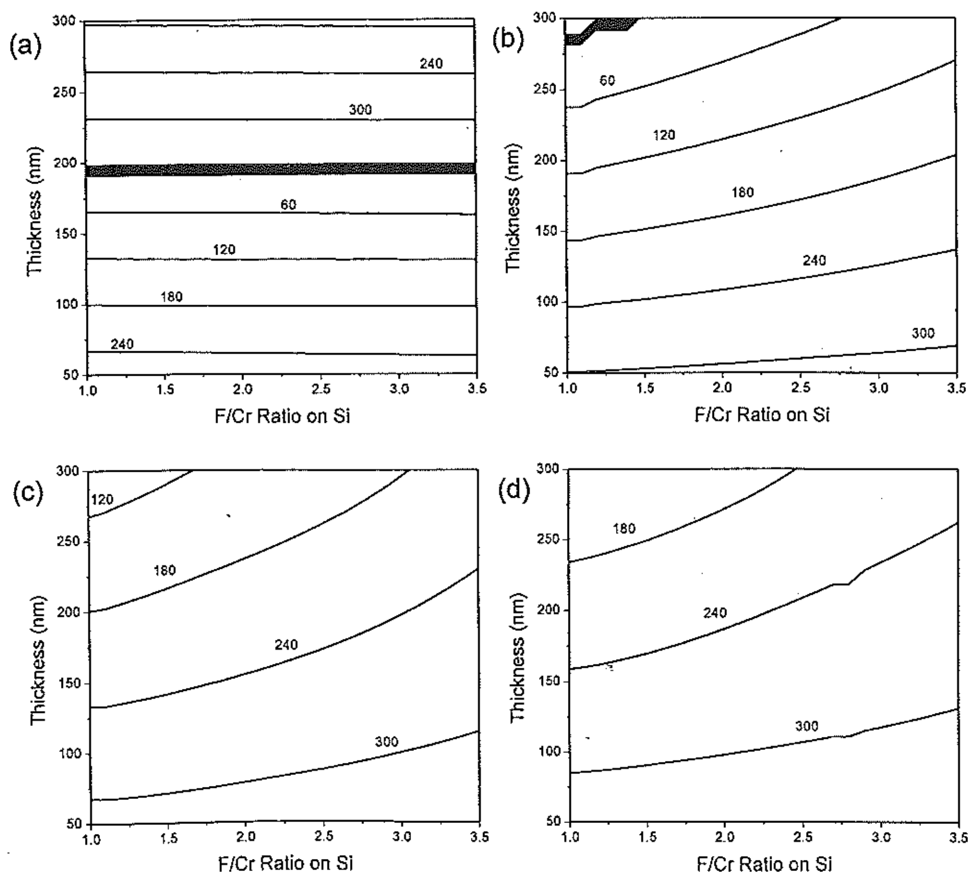

Fig. 11. Simulation of phase shift (numbers on the lines) over film thickness and film composition at wavelengths of (a) 193, (b) 248, (c) 365, and (d) 436 nm.

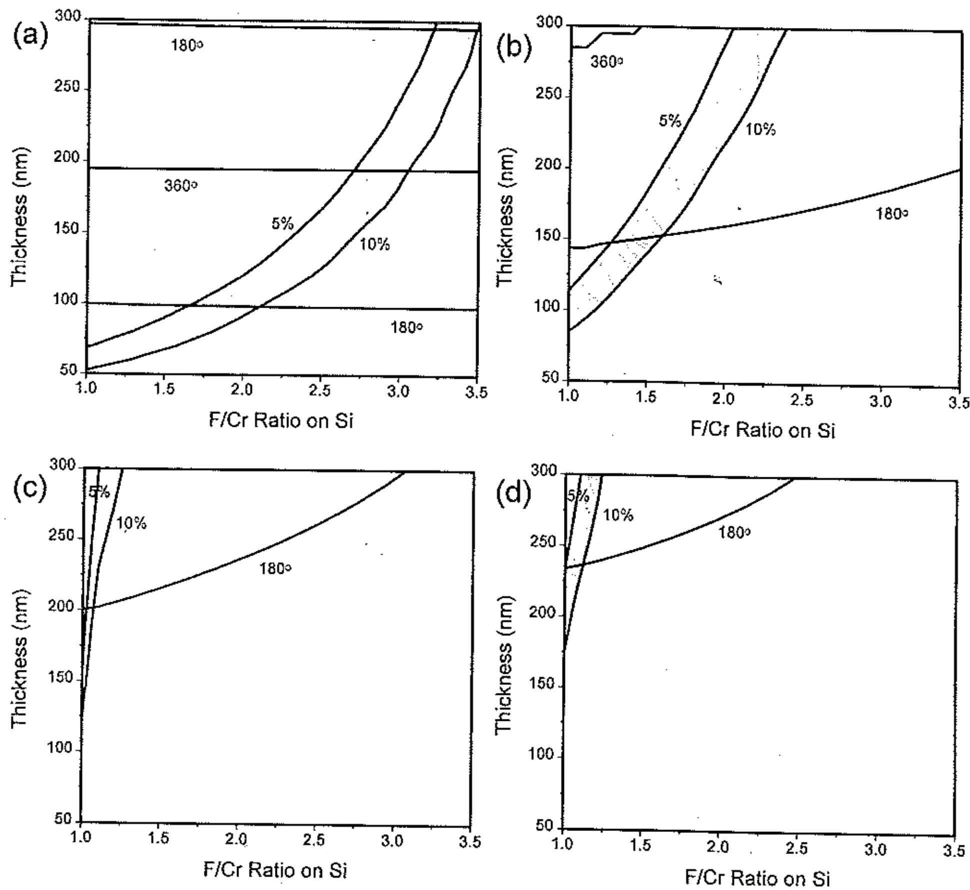

Fig. 12. Simulation of the Att-PSM fabrication condition at wavelengths of (a) 193, (b) 248, (c) 365, and (d) 436 nm.

efficient, because the fluorine strongly attracts electrons, making the electron transition more difficult.

Measured extinction coefficients at four different wavelengths are shown in Fig. 9. The extinction coefficient decreases exponentially as the composition ratio of F/Cr increases.

E. Simulation for Att-PSM Fabrication

1. *Simulation of Transmittance and Phase Shift*

From Figs. 8 and 9, if the film composition is known, the n and k values can be predicted in the range of F/Cr = 1–3.5. Therefore, only from the two given variables, i.e., composition and thickness, can we calculate the transmittance and the phase-shift contour plots, as shown in Figs. 10 and 11, respectively, using the equations mentioned in Subsections 2.B.

From the simulation results of transmittance in Fig. 10, the following facts can be induced. First, as the film thickness increases, the transmittance decreases, because, as the film thickness increases, the absorption distance of the incident light becomes longer. Second, with increasing fluorine content in the film, the transmittance increases. Because the electronegativity of the fluorine is so high, as mentioned in Subsection 4.D.2, its increasing content makes the electron transition more difficult, resulting in less absorption of the incident light. Third, the transmittance lines on the figure show more bending as the exposure wavelength increases. That is, the change of transmittance with the film thickness deviates from the monotonous exponentially decreasing trend. As the exposure wavelength increases, the available energy of electron excitation becomes less, causing a decrease in the extinction coefficient, and this in turn enhances the multiple reflection. As a result, the bending effect of the transmission lines becomes more eminent. Finally, as the fluorine content inside the film increases, the bending of the transmittance lines shows more bending. The increase of fluorine makes the transition of the electron difficult. This

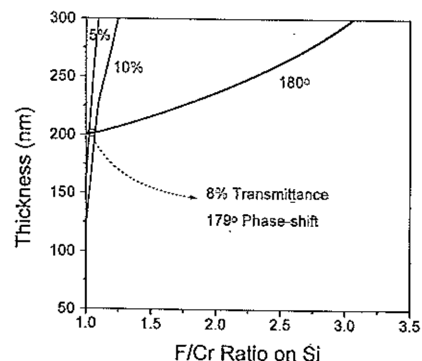

Fig. 13. Verification of the simulation at a wavelength of 365 nm. (The circled point is the data for verification.)

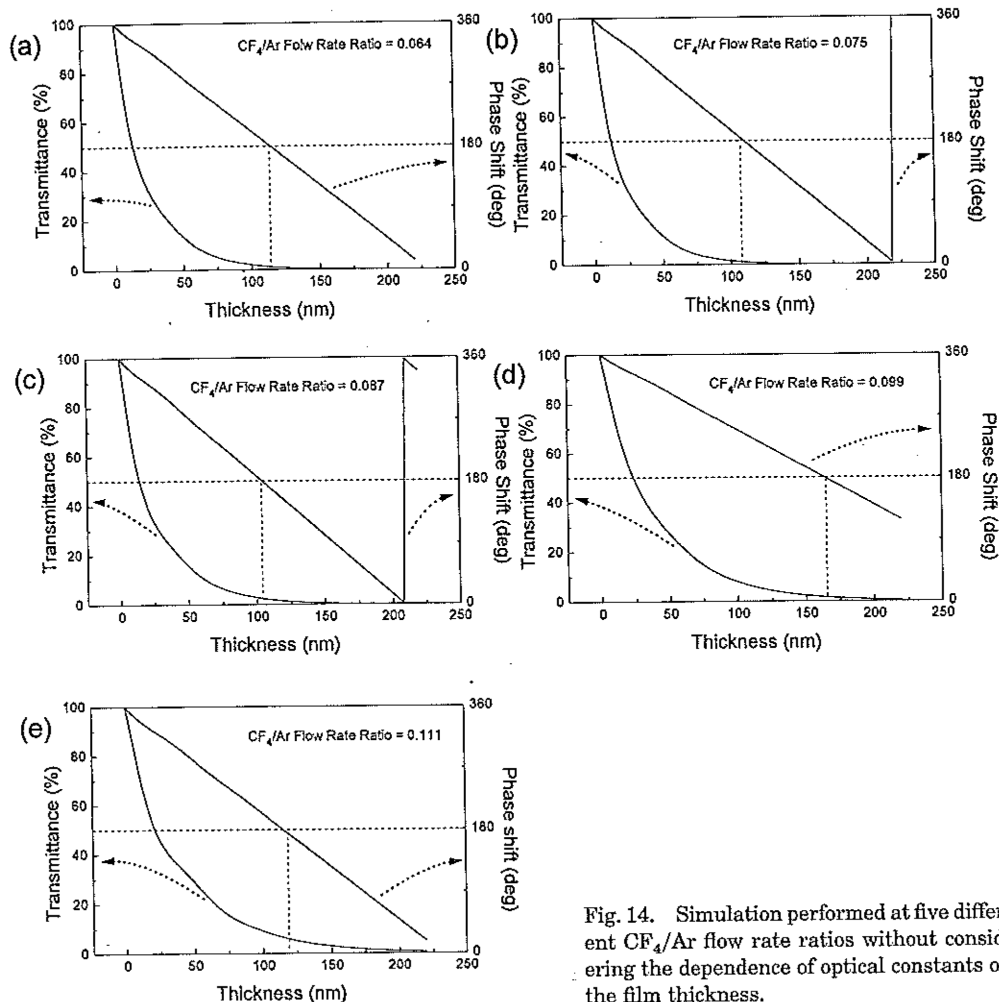

Fig. 14. Simulation performed at five different CF_4/Ar flow rate ratios without considering the dependence of optical constants on the film thickness.

results in a decrease in the extinction coefficient, which contributes to the multiple reflection.

The phase-shift simulation results in Fig. 11 can be explained as follows. When we describe the light as an electromagnetic wave and denote it as a phasor in the complex coordinate, the complex refractive index is multiplied by an imaginary number in the exponential term. As a result, the refractive index n becomes the imaginary part, so as to affect the phase shift. However, the extinction coefficient k becomes the real part, so as to affect the amplitude of the phasor. Therefore, as we can see from Fig. 8, at the longer wavelength region where the change of the refractive index with film composition is steeper, the change in phase shift with film thickness becomes more prominent. Besides, from the phase-shift relationship, $\varphi \cong (2\pi n d)/\lambda$, it is seen that $\lambda \Delta\varphi \propto \Delta d$. Therefore, with a constant $\Delta\ \varphi$, as λ increases, Δd increases. The linewidth in Fig. 11(d) is larger than that in Fig. 11(a). Similarly, because $\Delta\ \varphi \propto \Delta n \propto \Delta C$ (C is the composition ratio in terms of F/Cr), $\Delta\varphi$ increases as ΔC increases at the same wavelength.

2. *Optimum Att-PSM Fabrication Condition*

From the intersection of those two simulated plots, we can obtain the optimum Att-PSM condition having a transmittance of 5–10% and a phase shift of 180 deg, as shown in Fig. 12. Therefore the optimum film conditions for the Att-PSM are F/Cr = 1.64 ~ 2.07 and d = 100 nm or F/Cr = 3.2 ~ 3.45 and d = 295 nm at 193 nm, F/Cr = 1.10–1.35 and d = 124 nm at 248 nm, F/Cr = 1.02–1.08 and d = 201 nm at 365 nm, and F/Cr = 1.0–1.11 and d = 233 nm at 436 nm.

F. Verification of the Simulation

1. *Comparison between Simulated and Measured Values of Transmittance and Phase Shift*

The calculated result of transmittance and phase shift is verified by measuring the transmittance, phase shift, thickness, and composition of the films being deposited on the fused silica substrate. The films were made with various film thicknesses and compositions. As a result, we found that the results matched the simulated values within a 5% error range at wavelengths of 248 and 365 nm. However, we have no available exposure system, for the 193-nm wavelength, so we cannot verify at the 193-nm range. Nevertheless, because the simulation matches with the results at the other wavelength, it seems feasible that the simulation at the 193-nm wavelength would work as well.

2. *Att-PSM Fabrication*

Based on the results in Fig. 12, we fabricated the Att-PSM for the 365-nm wavelength. As a result, we obtained a CrF_x Att-PSM having an 8% transmittance and a 179-deg phase shift, as shown in Fig. 13.

G. Comparison with the Conventional Simulation Method

Usually it is assumed that optical properties such as n and k are independent of film thickness. However, as mentioned in Subsection 4.C, they are functions of film thickness. Therefore conventional simulation methods based on the assumption that optical constants are not a function of film thickness is not applicable in this study. For a direct comparison, the simulation was performed by conventional methods from the data of flow rate ratio variation experiments (Subsection 4.D) at the 193-nm wavelength, as shown in Fig. 14. According to Fig. 14, we can find the optimum Att-PSM fabrication condition at the 193-nm wavelength, when we choose the CF_4/Ar flow rate ratio to be 0.11 and the film thickness to be 115.3 nm.

Note that the optimum condition obtained by the conventional method differs from that of this study. Consequently, to yield more accurate data, the thickness effect on the optical properties should be taken into account in the Att-PSM simulation.

5. Summary

We have performed a simulation study of CrF_x films for an Att-PSM, considering three factors: the multiple reflection within both the film and the substrate, the dependence of optical constants on film thickness, and the thickness of the air layer having the same thickness as the film. As a consequence, we acquired the optimum conditions as $F/Cr = 1.64 \sim 2.07$ and $d = 100$ nm or $F/Cr = 3.2 \sim 3.45$ and $d = 295$ nm at 193 nm, $F/Cr = 1.10 \sim 1.35$ and $d = 124$ nm at 248 nm, $F/Cr = 1.02 \sim 1.08$ and $d = 201$ nm at 365 nm, and $F/Cr = 1.0 \sim 1.11$ and $d = 233$ nm at 436 nm. Moreover it was found that the simulation results agreed with the experimental results quite well. Therefore we suggest that the simulation performed in this study can be applied to other materials as well.

References

1. M. D. Levenson, N. S. Viswanathan, and R. A. Simpson, "Improving resolution in photolithography with a phase-shifting mask," IEEE Trans. Electron Devices **ED-29,** 1828–1836 (1982).
2. N. Hayashi, Micro Products Research Laboratory, Micro Products Division, Dai Nippon Printing Company, Ltd. 2-2-1 Fukuoka, Kamifukuoka, Saitama 356, Japan (personal communication, 1996).
3. S. Ito, H. Hazama, T. Kamo, H. Miyazaki, H. Sato, K. Hayashi, H. Shigemitsu, and I. Mori, "Optimization of optical properties for single-layer halftone masks," in *Optical/Laser Microlithography VII*, T. A. Brunner, ed., Proc. SPIE **2197,** 99–110 (1994).
4. H. Tanabe, J. Ushioda, and U. Seki, "Chromium fluoride attenuated phase-shift mask for ArF excimer laser lithography," in *Proceedings of Second International Symposium on 193nm Lithography* (Sematech, Colorado Springs, Colo., 1996), pp. 89–90.
5. L. F. Thompson, C. Grant Willson, and M. J. Bowden, *Introduction to Microlithography*, 2nd ed. (American Chemical Society, Washington, D.C., 1994), pp. 78–81.
6. B. J. Lin, "The attenuated phase-shifting mask," Solid State Technol. 42–47 (January 1992).
7. M. Bass, *Handbook of Optics*, 2nd ed. (McGraw-Hill, New York, 1995), Chap. 42.3.
8. S. M. Rossnagel, J. J. Cuomo, and W. D. Westwood, *Handbook of Plasma Processing Technology* (Noyes Publications, Park Ridge, N.J., 1990), Chap. 9.
9. S. Hong, E. Kim, Z.-T. Jiang, K. No, S.-C. Lim, S.-G. Woo, and Y.-B. Koh, "Effects of gas ring position and mesh introduction on film quality and thickness uniformity," Mat. Sci. Eng. B **45** (1–3), 98–101 (1997).
10. Z.-F. Zhou and Y.-D. Fan, "Stress and stress anisotropy in Co–Cr magnetic thin films deposited by magnetron sputtering," Thin Solid Films **272,** 43–48 (1996).
11. A. E. Ennos, "Stresses developed in optical film coatings," Appl. Opt. **5,** 51–61 (1996).
12. B. M. Mahan and R. J. Myers, *University Chemistry*, 4th ed. (Benjamin/Cummings, Menlo Park, Calif., 1975), pp. 661–664.